Environmental Pollution 263 (2020) 114390

Contents lists available at ScienceDirect

Environmental Pollution

journal homepage: www.elsevier.com/locate/envpol

High-resolution simulation of local traffic-related NO_x dispersion and distribution in a complex urban terrain☆

Xiangwen Fu [a, b], Songlin Xiang [a], Ying Liu [c], Junfeng Liu [a, *], Jun Yu [d], Denise L. Mauzerall [b, e], Shu Tao [a]

[a] Laboratory for Earth Surface Processes, College of Urban and Environmental Sciences, Peking University, Beijing, 100871, China
[b] Woodrow Wilson School of Public and International Affairs, Princeton University, Princeton, NJ, 08544, USA
[c] School of Statistics, University of International Business and Economics, Beijing, 100029, China
[d] School of Resources and Environmental Engineering, East China University of Science and Technology, Shanghai, 200237, China
[e] Department of Civil and Environmental Engineering, Princeton University, Princeton, NJ, 08544, USA

ARTICLE INFO

Article history:
Received 7 August 2019
Received in revised form
13 March 2020
Accepted 14 March 2020
Available online 16 March 2020

Keywords:
Emission
Human exposure
Street canyon
Spatial heterogeneity
Ventilation

ABSTRACT

Urban air pollution features large spatial and temporal variations due to the high heterogeneity in emissions and ventilation conditions, which render the pollutant distributions in complex urban terrains difficult to measure. Current urban air pollution models are not able to simulate pollutant dispersion and distribution at a low computational cost and high resolution. To address this limitation, we have developed the urban terrain air pollution (UTAP) dispersion model to investigate, at a spatial resolution of 5 m and a temporal resolution of 1 h, the distribution of the local traffic-related NO_x concentration at the pedestrian level in a 1×1 km^2 area in Baoding, Hebei, China. The UTAP model was shown to be capable of capturing the local pollution variations in a complex urban terrain at a low computational cost. We found that the local traffic-related NO_x concentration along or near major roads (10–200 $\mu g\ m^{-3}$) was 1–2 orders of magnitude higher than that in places far from roads (0.1–10 $\mu g\ m^{-3}$). Considering the background pollution, the NO and NO_2 concentrations exhibited similar patterns with higher concentrations in street canyons and lower concentrations away from streets, while the O_3 concentration exhibited the opposite behavior. Sixty percent of the NO_x concentration likely stemmed from local traffic when the background pollution level was low. Both the background wind speed and direction substantially impacted the overall pollution level and concentration variations, with a low wind speed and direction perpendicular to the axes of most streets identified as unfavorable pollutant dispersion conditions. Our results revealed a large variability in the local traffic-related air pollutant concentration at the pedestrian level in the complex urban terrain, indicating that high-resolution computationally efficient models such as the UTAP model are required to accurately estimate the pollutant exposure of urban residents.

1. Introduction

Urban areas, especially in developing countries, are often characterized by a combination of numerous buildings, a high population density, and severe air pollution. Consisting of buildings with various geometries, urban terrains are often highly complex and notably impact the local air quality and hence public health by influencing the airflow in the atmospheric boundary layer (Carpentieri et al., 2009; Gallagher, 2016; Krecl et al., 2015; Lateb et al., 2016; Zhong et al., 2018). Consequently, the dispersion of air pollutants in urban areas is a topic of active research in environmental science.

Street canyons are narrow streets lined with buildings along both sides (Vardoulakis et al., 2003) and are ubiquitous in urban built environments. At the street scale, the airflow and pollutant dispersion inside a street canyon are strongly associated with the canyon geometry (e.g., the aspect ratio (the ratio of the canyon height to the canyon width), the ratio of the building heights along

☆ This paper has been recommended for acceptance by Admir Créso Targino.

* Corresponding author. College of Urban and Environmental Sciences, Peking University, Beijing, 100871, China.
E-mail address: jfliu@pku.edu.cn (J. Liu).

https://doi.org/10.1016/j.envpol.2020.114390
0269-7491/

both sides of the canyon, etc.) (Baratian-Ghorghi and Kaye, 2013; Farrell et al., 2015; Gu et al., 2011). In addition, many other factors, including background wind conditions (Kwak et al., 2016; Solazzo et al., 2011), ground heating (Li et al., 2012), traffic flow (Thaker and Gokhale, 2016) and vegetation cover (Abhijith et al., 2017), also influence local pollutant dispersion. At the urban scale, complex street networks result in a high spatial ventilation heterogeneity. Urban air pollutant sources are also spatially heterogeneous. Based on high-resolution measurements, large spatial variabilities of air pollutants have been encountered in many urban areas (Li et al., 2018; Pattinson et al., 2014; Targino et al., 2018, 2016; Zhou and Lin, 2019). For example, the concentration variations of NO_x and black carbon could be as high as 5- to 8-fold even within the same street due to local emissions (Apte et al., 2017). The large variabilities in both emissions and ventilation conditions make it difficult to accurately characterize the spatial pattern of urban air pollution. Major urban air pollutants include CO, NO_x, SO_2, volatile organic carbon (VOC), O_3, PM_{10}, and $PM_{2.5}$. Human exposure to these pollutants results in adverse health impacts (e.g., pulmonary and cardiovascular diseases) and premature mortality (Burnett et al., 2018; Schraufnagel et al., 2019a, 2019b). Models with a low spatial resolution have been found to not be capable to capture the street canyon effect and might significantly underestimate human exposure levels to air pollutants (especially primary pollutants such as NO_x and black carbon) (Fallah-Shorshani et al., 2017b). Therefore, high-resolution model simulations of urban airflow and pollutant dispersion would enable the improved assessment of pollutant exposure and facilitate urban planning that provides better ventilation conditions and reduces air pollutant exposure and its associated adverse health impacts.

Street-scale air pollution simulations have been performed with empirical (e.g., land-use regression (LUR) models (Hankey et al., 2017; Patton et al., 2017; Weissert et al., 2018)), semiempirical models (e.g., the operational street pollution model (OSPM) (Brasseur et al., 2015; Lazić et al., 2016), the atmospheric dispersion modeling system (ADMS) (Barnes et al., 2014), the Research LINE (RLINE)-source (Patterson and Harley, 2019), SIRANE (Fallah-Shorshani et al., 2017a; Soulhac et al., 2016), AirGIS (Khan et al., 2019)) and numerical models (e.g., computational fluid dynamics (CFD) models (Aristodemou et al., 2018; Wang et al., 2019; Zhong et al., 2017)). Although LUR models consider many factors (e.g., traffic, land use, population, meteorological variables), they are based on numerous measurements, do not include chemistry and generally reflect the long-term average pollutant distribution (Hoek et al., 2008). Semiempirical models essentially rely on Gaussian dispersion modeling, include simple chemistry and can simulate the air pollution concentration at a low computational cost. However, semiempirical models either only consider the single-street canyon effect or have difficulty capturing the concentration variations inside a street (Buchholz et al., 2013; Soulhac et al., 2011; Wang et al., 2016a). CFD models are suitable for accurately calculating the pollutant dispersion and chemistry in complex urban terrains, but their simulation capabilities are limited by the high time consumption (Cheshmehzangi, 2016; Kwak et al., 2015; Vardoulakis et al., 2003). Thus, current models are not well suited to simulate urban-scale air pollutant dispersion at a high resolution at an acceptable computational cost. In this paper, we built on previous work by Fu et al. (2017) and developed an urban terrain air pollution (UTAP) model by combining CFD and Gaussian dispersion approaches and balancing the modeling accuracy and computational cost. We then applied the UTAP model to investigate the high-resolution dispersion and distribution of the local traffic-related NO_x concentration at the pedestrian level in a complex urban terrain.

2. Methods

2.1. Multiscale air pollutant dispersion modeling system

The UTAP model combines CFD and Gaussian models by adopting the CFD model to simulate the wind field in urban areas and then applying the Gaussian dispersion model to simulate the pollutant distribution based on the CFD-modeled wind field. Through this approach, the UTAP model is able to capture the influence of multiple buildings on pollutant dispersion at a high resolution while substantially reducing the computational time and providing better predictions than semiempirical models with a greater potential to conduct large-scale simulations in the future than CFD models.

We applied our model to Baoding, a densely populated, major city in Hebei, China. Baoding is adjacent to Beijing and the Xiongan New Area, is a major contributor to the air pollution in the Beijing-Tianjin-Hebei region and serves as a representative city in our study (Jiang and Bai, 2018). Considering the computational cost, in this paper, we adopted a 1×1 km^2 domain in downtown Baoding to demonstrate the capability of the UTAP model to accurately conduct high-resolution simulations. This domain consists of several roads and a large number of buildings (see Fig. S1). There is no local industrial source in the domain, and no high-resolution residential emissions data are available. Compared to the transportation contribution in Hebei Province, the residential contribution to NO_x is minor (Liu et al., 2016), and we focused on local traffic-related NO_x pollution (purely attributed to the traffic sources within the 1×1 km^2 domain) and investigated its spatiotemporal patterns.

As microscale air pollution modeling requires information on the background meteorological conditions and pollutant concentration, a microscale CFD model is commonly coupled with a mesoscale atmospheric model (Kwak et al., 2015; Michioka et al., 2013). In this paper, a multiscale air pollutant dispersion modeling system was built (Table S1). At the regional and urban scales, the mesoscale Weather Research and Forecasting (WRF) model (https://www.mmm.ucar.edu/weather-research-and-forecasting-model) was adopted to derive the meteorological fields for the Beijing-Tianjin-Hebei region and downtown Baoding (an area of 30×30 km^2). These two domains are illustrated in Fig. S2. At the street scale, the UTAP model was employed to simulate the fine-grid pollutant dispersion in the 1×1 km^2 domain at a spatial resolution of 5 m. The central longitude and latitude, grid resolution and number of grids in the three domains are summarized in Table S1.

The urban canopy model (UCM) is a widely used module embedded in the WRF model to better characterize the influence of the urban canopy on the meteorological conditions and atmospheric chemistry in the urban environment (Li et al., 2017; Wang et al., 2016b). We applied the single-layer urban canopy model (SLUCM) (Chen et al., 2011) to our simulations to derive the background wind conditions of the 1×1 km^2 domain as input to the UTAP model. Based on the GIS map of Baoding, we classified the land use of downtown Baoding as a high-intensity residential area. We adopted the urban parameters for the Beijing-Tianjin-Hebei region of Barlage et al. (2016), as indicated in Table S2.

2.2. Wind database based on the parallelized large-eddy simulation (LES) model (PALM)

Large-eddy simulation (LES) is a commonly favored approach in CFD models to solve complex turbulent flows (Vardoulakis et al., 2003; Zhong et al., 2015). LES is computationally efficient because it only explicitly resolves large eddies while parameterizing small

eddies, making it faster than direct numerical simulation (DNS). In addition, it is able to capture flows at high temporal and spatial resolutions and is thus more accurate than the Reynolds-averaged Navier-Stokes (RANS) approach (Aristodemou et al., 2018; Hang et al., 2017). We adopted the parallelized LES model (PALM) (Maronga et al., 2015) to derive the three-dimensional wind fields in the 1 × 1 km^2 domain while considering the effect of buildings. PALM is capable of conducting parallelized computation and has been proven to perform well for urban terrains (Park et al., 2015b, 2015a). The surface topography was extracted from online map resources. Applying the method of Park et al. (2015a, b), buffer regions (consisting of artificial buildings arranged in lines, as shown in Fig. 1) were added around the 1 × 1 km^2 domain to prevent turbulence from abrupt dissipation near the lateral boundary. The turbulence recycling method (Maronga et al., 2015) was employed during the simulations to generate turbulent inflows for the domain of interest, and a recycling domain was added to the upstream area (indicated in Fig. 1).

With 360 possibilities of background winds, i.e., the boundary wind conditions of the 1 × 1 km^2 domain of Baoding (5 wind speeds × 72 wind directions, and the values at a height of 10 m are listed in Table S3) as inputs, we ran PALM and compiled a wind database of 360 possible three-dimensional wind fields for the domain with an area of 1 × 1 km^2 and a height of 300 m at a spatial resolution of 5 m (i.e., 200 × 200 grid points in the horizontal dimension and 60 grid points in the vertical dimension). When setting the background winds, we adopted the empirical wind profile as defined below, which follows a power law (Jiang et al., 2004):

$$\begin{cases} u_2 = u_1\left(\frac{z_2}{z_1}\right)^m, \ z_2 \le 200m \\ u_2 = u_1\left(\frac{200}{z_1}\right)^m, \ z_2 > 200m \end{cases} \quad (1)$$

where u_1 (known value, e.g., the measured data) and u_2 represent the wind speeds at heights of z_1 and z_2, respectively, and m is the exponential factor (see Table S4 for the values used (Jiang et al., 2004)). For each background wind, we ran PALM for an hour and included the averaged wind field in the database.

2.3. Major processes in the UTAP model

2.3.1. Emission

We assume that all traffic pollutant emissions are emitted from the 10 major road segments in the 1 × 1 km^2 domain. The UTAP model reads the emissions (see Section 2.4 for details on determining the traffic emissions) based on a road matrix (5-m resolution, as shown in Fig. S3). Every grid point in the road matrix belonging to a road acts as a traffic point source in the model. The emissions along each road are evenly distributed across these point sources.

2.3.2. Dispersion and dry deposition

According to the background wind condition input derived from the WRF model, the UTAP model selects two wind fields from the PALM wind database whose background wind conditions are the closest to those of the input, and the wind field is then generated by interpolation.

Following our previous work, the process of pollutant dispersion in the UTAP model is similar to the model described in Fu et al. (2017). Gaussian puffs are emitted from traffic sources and then move and disperse in the urban wind field until leaving the domain. Upon hitting the ground and building walls, the reflection and dry deposition of the puffs are calculated. The dry deposition of air pollutants is simulated according to the equation below:

$$\frac{dC_i}{dt} = -\frac{V_{d,i}}{z} \times C_i \quad (2)$$

where C_i is the pollutant concentration, $V_{d,i}$ is the deposition velocity, and z is the height across which the air is well mixed (assumed to be 5 m, i.e., the model resolution). The deposition velocity is adopted from Su et al. (2010).

2.3.3. Chemistry

In terms of the atmospheric chemistry, since the pollutant

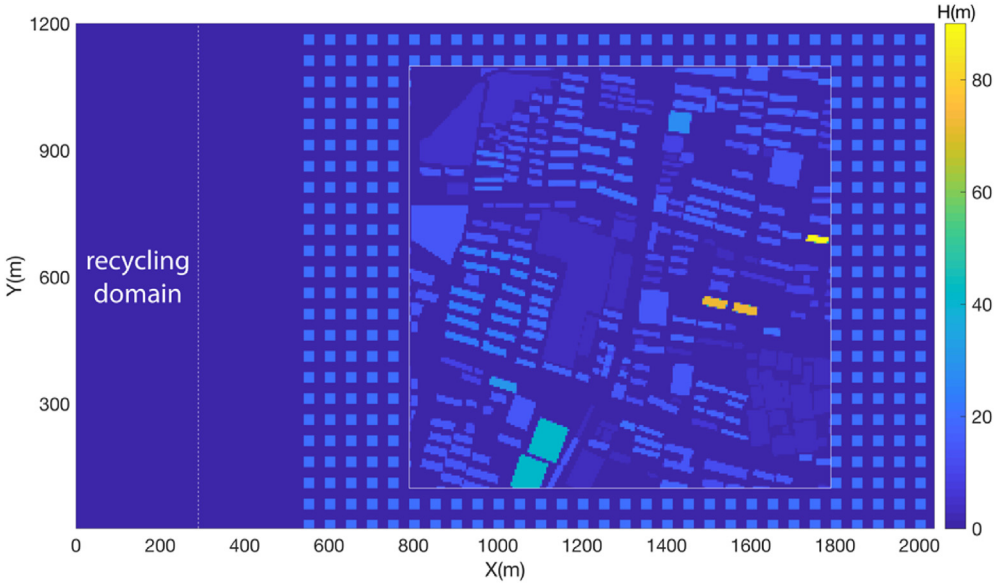

Fig. 1. Illustration of the surface topography in PALM. The 1 × 1 km^2 domain is indicated by the inner square with the white solid lines. The color indicates the elevation of the buildings. The recycling domain is to the left of the dashed line. (For interpretation of the references to color in this figure legend, the reader is referred to the Web version of this article.)

dispersion within the street canyons is on a timescale ranging from seconds to minutes, previous semiempirical models (Silver et al., 2013; Soulhac et al., 2011; Venegas et al., 2014) generally focused on the fast reactions of NO_x and O_3. In the UTAP model, we followed the SIRANE method, which treats NO_x (NO and NO_2) as an inert species during dispersion modeling and then calculates the equilibrium concentrations of NO, NO_2 and O_3. O_3 initially comes from the background atmosphere and reacts with the locally emitted NO and NO_2 based on the mechanism below (Soulhac et al., 2011):

$$\begin{cases} NO_2 + h\nu \xrightarrow{k_1} NO + O\cdot & (R1) \\ O\cdot + O_2 \xrightarrow{k_2} O_3 & (R2) \\ NO + O_3 \xrightarrow{k_3} NO_2 + O_2 & (R3) \end{cases}$$

2.4. Model evaluation

We evaluated the UTAP model against measurements obtained in the 1×1 km^2 domain of Baoding. The hourly wind speed, wind direction and NO_x concentration were measured by two roadside monitoring stations (denoted as S1 and S2 in Fig. S4) between December 22, 2017 at 14:00 and December 25, 2017 at 14:00, which is a time interval when the air pollution in winter is severe (see Section S3 for more details on the NO_x measurements). Each hour, we also counted the number of four types of vehicles (light-duty and heavy-duty passenger vehicles and light-duty and heavy-duty trucks) on the ten major roads in the domain during this time period using camera footage. The traffic emissions were estimated by multiplying the number of vehicles by the emission factors from Chen et al. (2016) (see Table S5).

Fig. 2 (and Fig. S5 for monitoring station S2) shows the observed and simulated wind speeds and directions at monitoring station S1. The results of WRF-UCM are included for comparison. Due to the spatial resolution of 1 km, the winds predicted by WRF-UCM were the same for the two stations. The ground-level wind speeds observed at the two stations were both below 1 m s^{-1} with little variation, reflecting a relatively stable atmosphere inside the street canyon. In contrast, the wind speeds simulated by WRF-UCM fluctuated sharply around 0–3 m s^{-1} and were generally higher than the observations, which demonstrates that the WRF model failed to precisely capture the ground-level wind speed in the urban environment. Compared to WRF-UCM, the wind speeds predicted by the UTAP model were much closer to the observations. The wind directions at S1 and S2 exhibited significant temporal variations and differed substantially from each other. While WRF-UCM could not differentiate between the different wind directions at the two stations, the UTAP model reflected the influence of the complex urban terrain on the wind directions at the two locations. At specific hours (e.g., during the mornings of 23 and 25 December), there were large discrepancies (approximately 90°–120°) between the observed and UTAP-simulated wind directions. These discrepancies may be due to the inaccurate background wind field simulation by WRF-UCM or uncaptured local turbulences around the monitoring stations. Overall, the UTAP model simulated the wind field well.

Fig. 3 shows the modeled and measured NO_x concentrations at the two stations. The concentrations simulated by PALM are also shown for comparison. The total concentrations in the UTAP model and PALM were obtained by summing the traffic contribution and the urban background pollution. The background NO_x concentration was estimated based on the data from the national air quality stations in Baoding. Both the pollution levels and diurnal variations in the concentrations were well reproduced by the two models. The Gaussian dispersion module in the UTAP model produced similar concentration results as those produced by PALM, while the UTAP model required much less computational time than PALM did (3 min versus 3 h to simulate a 1-h concentration distribution). Table 1 lists several performance measures of the air quality models and the background. The data show that the UTAP model and PALM

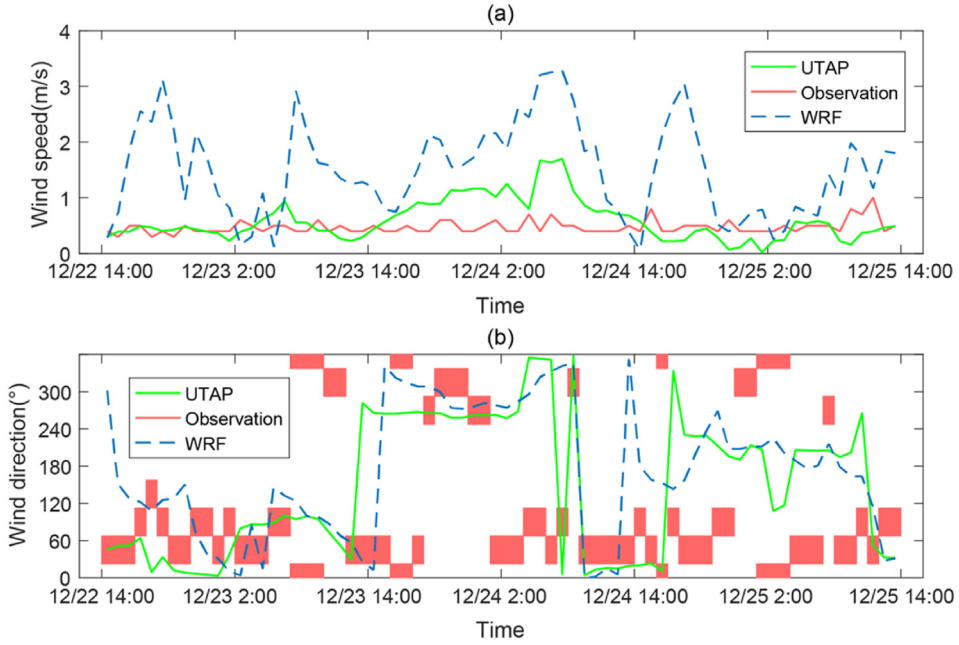

Fig. 2. Simulated and measured (a) wind speeds and (b) wind directions at monitoring station S1. The green solid lines, red solid lines/rectangles and blue dashed lines represent the UTAP simulation results, observations, and WRF-UCM data, respectively. The wind directions shown in the blocks as the observed directions are qualitative. The height of a block indicates the range of all possible quantitative wind directions corresponding to the observed direction. (For interpretation of the references to color in this figure legend, the reader is referred to the Web version of this article.)

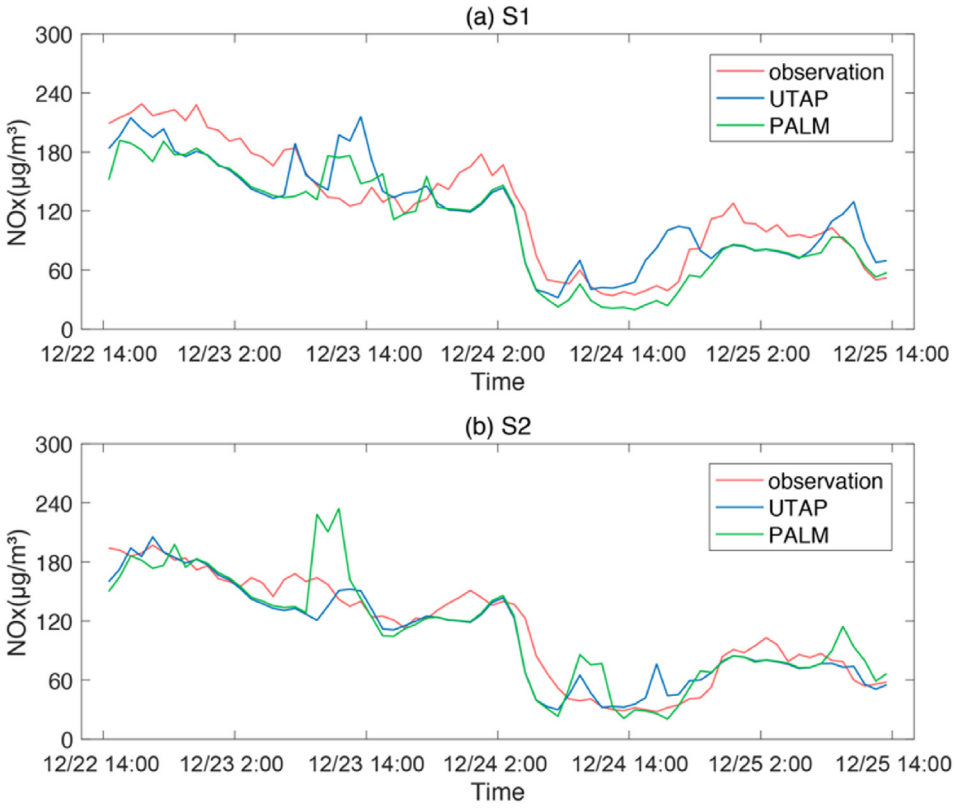

Fig. 3. The simulated and measured NO_x concentrations at (a) S1 and (b) S2 at a height of 2.5 m. The red, blue and green lines represent the observations and the UTAP and PALM simulation results, respectively. (For interpretation of the references to color in this figure legend, the reader is referred to the Web version of this article.)

Table 1
Summary of the performance measures for model evaluation regarding the NO_x concentration.

Performance Measures	Normalized Root Mean Square Error (NRMSE)	Fraction of C_e Within a Factor of 2 of C_o (FAC2)	Fraction Bias (FB)	Correlation Coefficient (R)
Definition	$NRMSE = \sqrt{\overline{(C_o - C_e)^2}}/\overline{C_o}$	Fraction where $0.5 < \frac{C_e}{C_o} < 2$	$FB = 2(\overline{C_o} - \overline{C_e})/(\overline{C_o} + \overline{C_e})$	$R = \overline{(C_o - \overline{C_o})(C_e - \overline{C_e})}/(\sigma_{C_o} \cdot \sigma_{C_e})$
Ideal Value	0	1	0	1
Urban Criterion	–	>0.3	(-0.67, 0.67)	–
UTAP, S1	0.25	0.97	0.05	0.84
PALM, S1	0.23	0.99	0.17	0.91
Background, S1	0.28	0.86	0.29	0.96
UTAP, S2	0.17	0.96	0.05	0.93
PALM, S2	0.23	0.93	0.01	0.87
Background, S2	0.20	0.89	0.17	0.95

C_o: observed concentration; C_e: estimated concentration; σ_{C_o}: the standard deviation of the observed concentration; σ_{C_e}: the standard deviation of the estimated concentration. The urban criteria for the performance measures are adapted from Chang and Hanna (2004).

both essentially performed equally well. This result also justified the simplified chemistry in the UTAP model at the street scale. Compared to the background, the UTAP model achieved further improvements, which means that combining the local traffic and background pollution levels in the UTAP model could better reflect the total NO_x pollution level in complex urban terrains.

3. Results and discussion

3.1. Wind fields in the complex urban terrain

Based on the PALM simulations, the UTAP model could generate the wind fields in the 1×1 km^2 domain in Baoding. Complicated airflow patterns were observed as air entered the street canyons with various geometric characteristics driven by the background wind (see Fig. S6). Horizontally, the wind directions were jointly determined by the background wind direction and the axes of the street canyons (Figs. S7a and b). Vertically, the street canyon effects (Vardoulakis et al., 2003) were captured by the UTAP model since the vortices within the street canyons drove the winds upward on the leeward side and downward on the windward side (Fig. S7c). Influenced by the underlying surface, the wind speed substantially decreased at a lower height (Figs. S7d–f).

3.2. Dispersion of the traffic-related NO_x

To study the dispersion of traffic-related primary pollutants in complex urban terrains, we applied the UTAP model to simulate the dispersion of NO_x emitted by the traffic sources in the 1×1 km^2 domain in Baoding over the period for which the model was

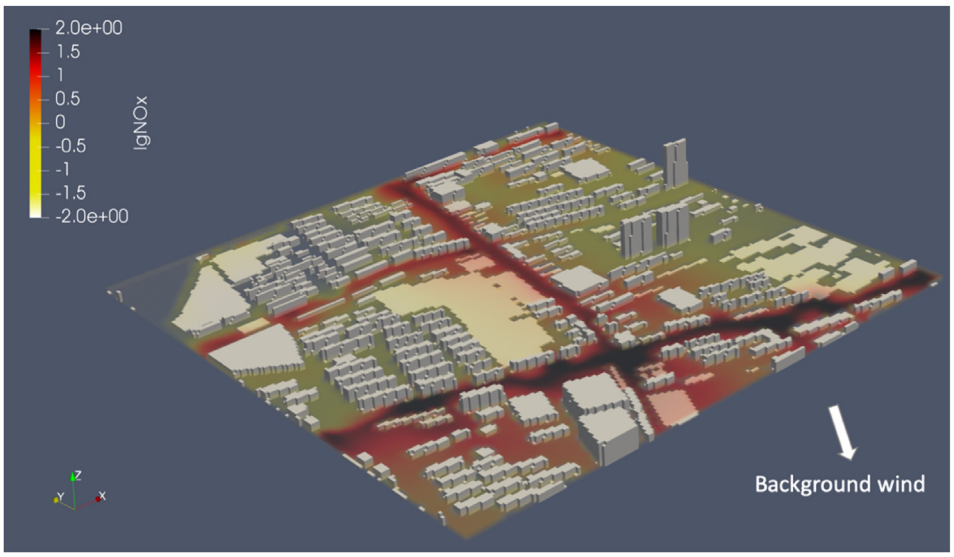

Fig. 4. Snapshot of the distribution of the local traffic-related NO_x concentration in the 1 × 1 km^2 domain in Baoding (unit: μg m^{-3}). The buildings are displayed in gray. The pollutant concentration is shown in colors of the "haze". The background wind direction is indicated by the white arrow. The simulation time is December 22, 2017 at 14:00. Note that the legend has a log scale. (For interpretation of the references to color in this figure legend, the reader is referred to the Web version of this article.)

evaluated. The background NO_x and O_3 concentrations were obtained from the national air quality stations in Baoding. The temporal and spatial resolutions were 1 h and 5 m, respectively. Fig. 4 shows a snapshot of the three-dimensional NO_x distribution in the domain, indicating that the spatial variation in the concentration could be over several orders of magnitude. The NO_x dispersion pattern was highly dependent on the background winds, street geometry and emission pattern (see Fig. S8). For streets with axes nearly perpendicular to the background winds, part of the pollutants accumulated inside the street canyons, while the remainder was removed from street canyons through the openings between buildings or moved above the street canyons and was further dispersed downwind. For streets with axes nearly parallel to the background winds, pollutants basically moved along the street canyons without notable transport between the streets. The pollution levels in the early hours (Fig. S8d) were much lower than those at the other times of the day due to the smaller number of vehicles on the road.

Fig. 5a shows the time-averaged distribution of the local traffic-related NO_x concentration at the pedestrian level (1.5 m) over the 3 days (the background wind rose during that time interval is illustrated in Fig. 5b). There were substantial spatial variations in the concentration. The pollution levels along the roads (10–200 μg m^{-3}) were 1–2 orders of magnitude larger than those in places away from the roads (0.1–10 μg m^{-3}). This difference in the pollution level was due to two reasons. First, the buildings along both sides of the streets hindered pollutant dispersion, keeping the vehicle-emitted NO_x inside the street canyons. Second, the Gaussian puffs diffused while moving, thus decreasing the traffic contribution to pollution in areas far away from the roads (negligible compared to the background NO_x concentration of 10–100 μg m^{-3} during the time of simulation). Along the different

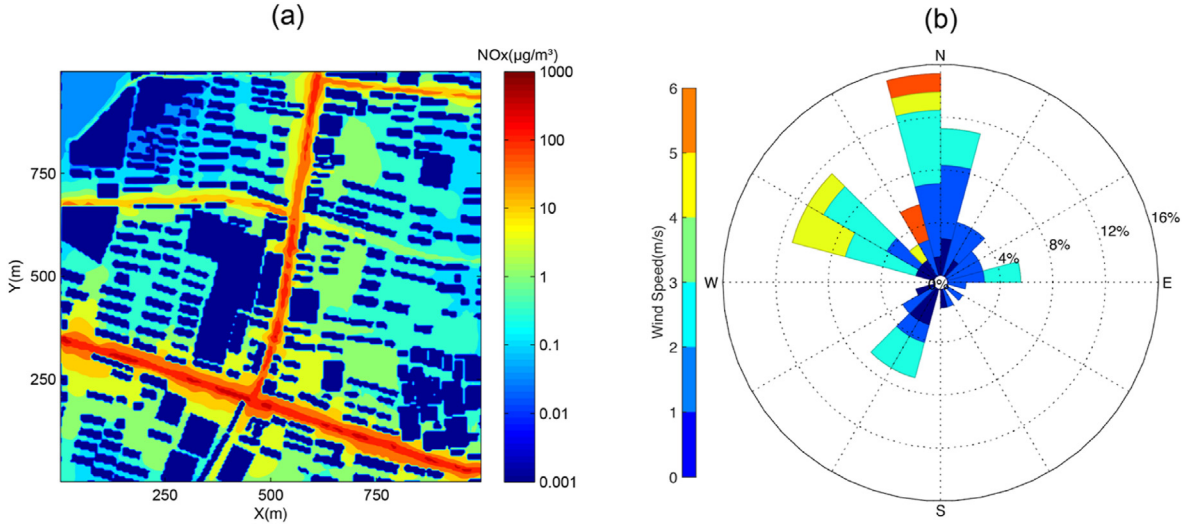

Fig. 5. The (a) time-averaged distribution of the local traffic-related NO_x concentration at the pedestrian level (1.5 m) and (b) background wind rose of the 1 × 1 km^2 domain in Baoding during the measurement period. Note that the legend in panel (a) has a log scale.

roads, the pollution level primarily also varied because of the difference in traffic volume. The spatial variations in NO_x were larger along or near the roads than elsewhere. This pattern was consistent with previous findings (Patton et al., 2014; Zhang et al., 2017), whereby distance-decay gradients were reported for traffic-related air pollutants from major roads.

3.3. Temporal and spatial distributions of the pollutant concentration

Fig. 6a depicts the temporal variations in the domain-averaged NO_x concentration at the pedestrian level over the 3 days. The variations in the traffic-related NO_x concentration generally depended on the temporal pattern of the traffic volume (high from 7:00 to 22:00 and nearly zero for the rest of the time). When the background pollution in Baoding was high, the local traffic-related NO_x concentration accounted for less than 20% of the total NO_x concentration. However, when the background air was relatively clean, local traffic contributed as much as 60% of the NO_x pollution in the domain. This result demonstrated the importance of local traffic-related pollution to the urban air quality. With the substantial efforts in China on pollution mitigation in the power and industrial sectors, the background NO_x pollution levels in urban areas will be lowered, and the significance of local traffic emissions on NO_x pollution will be greater. However, the traffic contribution may also decrease in the future due to the increased adoption of electric vehicles in China. As shown in Fig. 6b, the temporal variations in NO and NO_2 were similar to those in NO_x, while O_3 showed the opposite pattern due to its reactions with NO_x (Soulhac et al., 2011). During the hours with a high NO concentration (e.g., all of December 22 and 23 and the morning of December 25), the O_3 reaction with NO dominated and the ground-level O_3 concentration was nearly zero. When NO concentration decreased on December 24, NO_2 photolysis dominated instead, and the O_3 concentration increased to approximately 60 μg m^{-3}.

Fig. 7 shows the spatial distributions of the time-averaged pollutant concentration at the pedestrian level. With the urban background concentration considered, the pollutants still exhibited pronounced spatial variations. NO_x (NO and NO_2) pollution was heavier near the major roads. For NO_x and NO, the differences between the pollution levels along and away from the streets were very large (200 versus 100 μg m^{-3} for NO_x and 50 versus 30 μg m^{-3} for NO). NO_2 demonstrated a smoother concentration transition (80–100 μg m^{-3} along the streets and 70 μg m^{-3} away from the streets), since NO_2 is mainly a secondary species and has a lower spatial gradient. In contrast, the spatial distribution of the O_3 concentration was the opposite of that of the NO_x concentration. The O_3 concentration was lower along or near the roads, where most O_3 would be removed by the freshly emitted NO from the on-road vehicles through the process of NO_x titration (Kimbrough et al., 2017).

To evaluate air pollution and its health impacts on humans, many region-scale studies employed mesoscale atmospheric models with a resolution of tens of kilometers (Qin et al., 2017; Yang et al., 2018). However, to better estimate the exposure of urban residents to air pollutants (especially traffic-related pollutants), high-resolution simulations are recommended (Batterman et al., 2014). Although we can estimate the overall exposure level of the population with low-resolution models or measured data from tens of air quality stations, it remains difficult to accurately evaluate the exposure levels at various locations (especially those near the emission sources) in a city. The large uncertainties in external exposure would persist in the assessment of health impacts and the determination of air pollutant dose-response relationships. As indicated by our findings, there were notable variations in traffic air pollution between the ground and urban background levels and between the different locations in the complex urban terrain. Apart from traffic sources, urban industrial and residential sources might further add to the spatial variations of the pollutant concentration. The UTAP model considered the building geometry and captured the local variations of the concentration while remaining computationally efficient, which enables urban-scale high-resolution

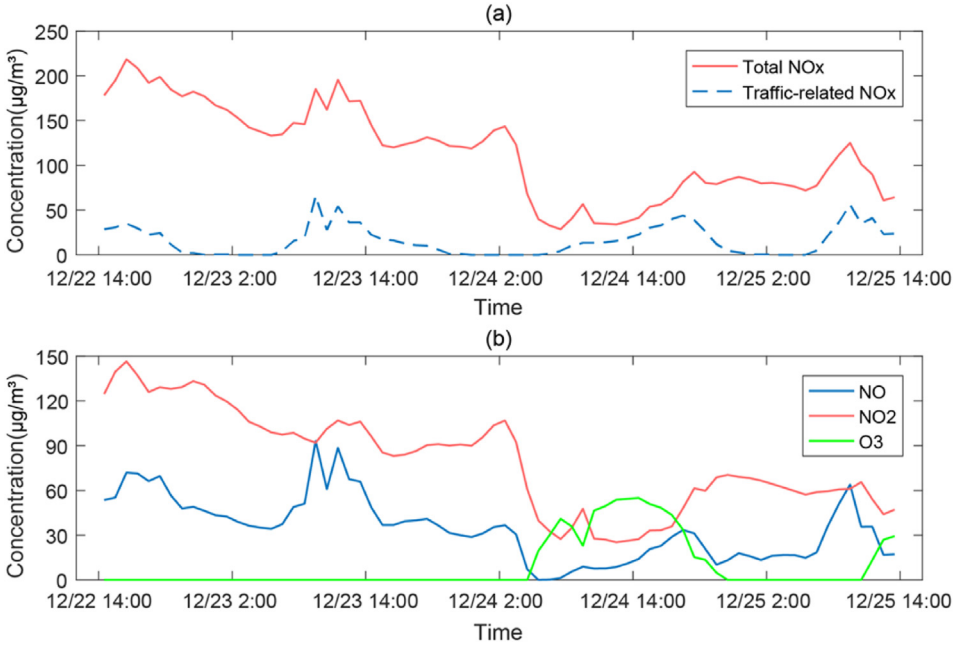

Fig. 6. The temporal variations in the domain-averaged pollutant concentration at the pedestrian level (1.5 m) in the 1 × 1 km^2 Baoding domain during the measurement period. In panel (a), the red solid line and the blue dashed line represent the total and local traffic-related NO_x concentration, respectively. In panel (b), the blue, red and green lines represent the total NO, NO_2 and O_3 concentrations, respectively. (For interpretation of the references to color in this figure legend, the reader is referred to the Web version of this article.)

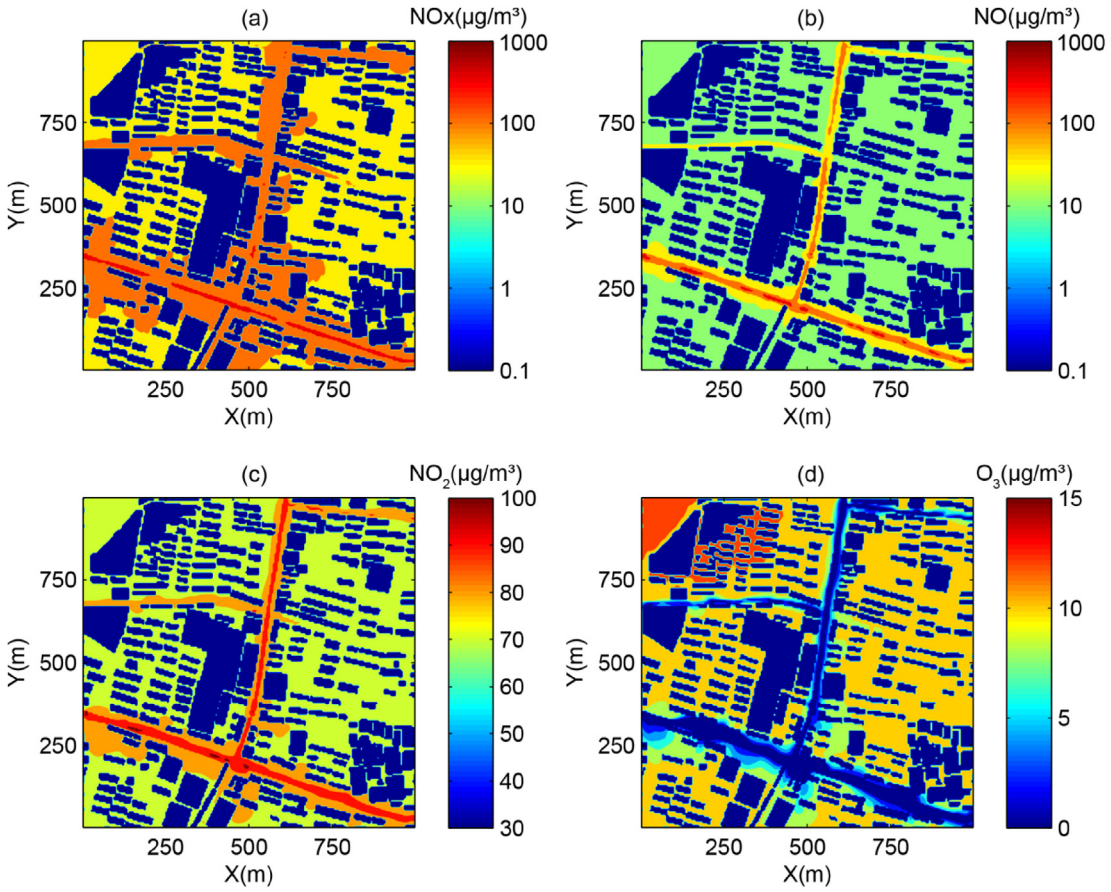

Fig. 7. The distribution of the time-averaged (a) NO_x, (b) NO, (c) NO_2, and (d) O_3 concentrations at the pedestrian level (1.5 m) in the 1 × 1 km^2 Baoding domain during the measurement period. Note that the legends are not the same for all panels.

applications. Therefore, it is important for future environmental and epidemiological studies to develop and use high-resolution atmospheric models such as the UTAP model in urban environments.

To improve the performance of urban dispersion models in evaluating air pollutant exposure, various sources of high-resolution data, including urban morphology, background meteorology and pollution, emissions inventory and population distribution, are required (Forehead and Huynh, 2018). There has been research on urban air pollution and exposure assessment incorporating big data. Messier et al. (2018) established a data-only approach and LUR-kriging model to efficiently exploit measured big data to map urban air pollution at a high resolution. Hankey et al. (2017) examined the possibility of lowering the population exposure to air pollutants through urban planning based on numerous traveling and pollution data. Future research would require more data to better predict the pollutant concentration and human exposure in complex urban terrains. For instance, by combining the traveling demand of urban residents, the UTAP model can be utilized to assess the real-time population exposure and achieve optimal travel route planning aimed at minimizing personal exposure.

3.4. Impacts of the background wind conditions on the local traffic-related NO_x pollution

In addition, to study the impact of the background wind conditions on the pollutant distribution in the domain, we modeled the pollutant dispersion under 360 typical background winds (the same as the input conditions when building the PALM wind database, as indicated in Table S2). Fig. 8a shows the domain-averaged local traffic-related NO_x concentration at the pedestrian level under the various background winds (Fig. 8b shows the standard deviation of the NO_x concentration). The background wind speed had a notable influence on both the average pollution level and the spatial variability of pollution. When the background wind was weak (i.e., <3 m s^{-1}), the domain-averaged NO_x concentration was much higher than that under strong background winds. When the background wind speed increased from 1 to 3 m s^{-1}, the average concentration decreased by more than 50%. In addition, relatively weak winds resulted in larger spatial variations in the NO_x concentration, which implies that the pollution in hotspots would be even more severe. Regarding the role of the wind direction, we found that although not as marked as the wind speed, the background wind direction also affected the pollutant distribution, especially in the low-wind speed cases. When the background wind speed was below 3 m s^{-1}, it was clear that the domain-averaged NO_x concentration and its standard deviation tended to be higher when the wind direction was approximately 20° (i.e., nearly perpendicular to the long axes of most buildings and the axes of the street canyons shaped by these buildings in the domain). In these cases, as the background wind entered the street canyons perpendicularly, the airflow formed vertical vortices inside the canyons, which led to poor ventilation conditions, high pollution levels and large spatial variations. This result implies that urban air pollution impacts could be reduced through urban planning considering the influence of the street geometry on ventilation conditions. For example, buildings oriented along the prevailing

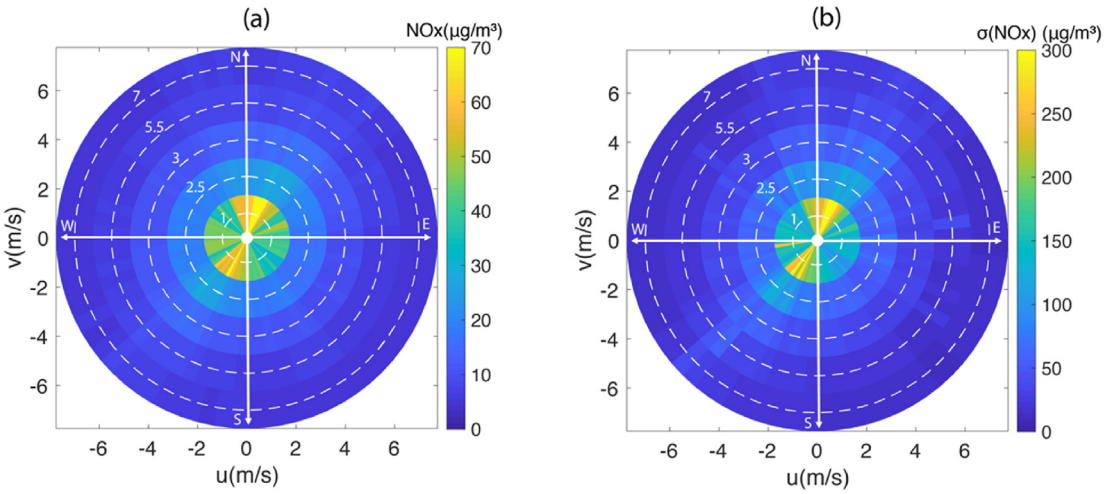

Fig. 8. The (a) domain average and (b) standard deviation of the local traffic-related NO_x concentration at the pedestrian level (1.5 m) in the 1 × 1 km^2 domain of Baoding as a function of the x- (west to east) and y- (south to north) components of the background wind. The total background wind speed (m/s) is marked by the dashed white circles.

local wind direction would effectively ameliorate the air quality on the whole and even more in the hotspots.

3.5. Caveats

Herein, we summarize the uncertainties of our simulation results.

First, our results were dependent on accurate predictions of the background meteorological and chemical conditions. For the meteorological conditions, we simulated the 3-day-averaged distribution of the local traffic-related NO_x concentration at the annually averaged air temperature of Baoding and obtained similar results (Section S1), which implies that the simulated pollutant dispersion in winter was representative of the annual average. The concentrations observed at the air quality stations in Baoding might be influenced by local pollution and serve as an unsatisfactory proxy of the urban background pollution level. Nevertheless, it would not affect our findings on the dispersion of the traffic-related NO_x.

Second, the performance of the UTAP model was directly affected by the quality of the emission data. Owing to the difficulties of obtaining a high-resolution emission inventory, the traffic emissions were estimated for only three days. The biases from either counting the vehicles or the adoption of emission factors would diminish the reliability of the simulated traffic emissions. Other pollution sources (e.g., industrial and residential sources) were not included due to lack of information, which also limits the model capability of evaluating the total external exposure of urban residents.

Third, certain parameters in the UTAP model may also have an impact on the simulated NO_x distribution. We performed a sensitivity test of the moving interval of the Gaussian puffs, which demonstrated that the current resolution of puff movement is necessary (Section S2).

Fourth, in this study, we focused on the influences of the background winds and of the complex urban terrain on the urban wind fields without considering traffic-induced turbulence, which could facilitate ventilation and lower the concentration gradient (Pospisil and Jicha, 2017). However, the scale and intensity of traffic-induced turbulence are often limited, depending on the number of vehicles and vehicle speed.

Additionally, the chemistry module in the UTAP model is the same as that in the SIRANE model, which simplifies the reactions between NO_x and O_3 by assuming that a chemical steady state is reached. Kimbrough et al. (2017) revealed that when applying Gaussian dispersion to the conversion of NO to NO_2, the availability of background O_3 should be considered. The simplified chemistry works well in winter but may not be adequate in summer, when biogenic hydrocarbons are released in vastly larger quantities and volatilization of anthropogenic hydrocarbons is more intense as well due to the higher temperature. This module will be improved in future research.

In addition, the UTAP model was validated using measurement data from only two sites in the 1 × 1 km^2 domain. Additional higher-resolution data will be collected to better examine the performance of the UTAP model.

4. Conclusions

In this study, we investigated the distribution of the local traffic-related NO_x concentration in a complex urban terrain. By developing a high-resolution urban dispersion model (the UTAP model), we simulated the pollutant distribution at the pedestrian level in a 1 × 1 km^2 domain in Baoding city in Hebei, China, for three days in December 2017 at a spatial resolution of 5 m and a temporal resolution of 1 h.

We found that the local traffic-related air pollutant dispersion and distribution in the urban area were greatly influenced by both the ventilation conditions and emissions. The ground-level urban wind fields were characterized by complex turbulence patterns and jointly determined by the background winds and street geometry. The local traffic-related NO_x concentration along the streets was 1–2 orders of magnitude higher than that elsewhere, with a concentration ranging from 10 to 200 μg m^{-3} along or near the major roads and a concentration ranging from 0.1 to 10 μg m^{-3} in places far away from the roads. We also observed that the total NO_x (as well as NO and NO_2 separately) concentration at the pedestrian level was higher along the roads, while the O_3 concentration exhibited the opposite spatial pattern because of NO_x titration. The absolute contribution of traffic to the NO_x concentration was determined by the temporal pattern of the traffic volume, while the relative traffic contribution also depended on the background pollution of Baoding and could reach as high as 60%.

For the impacts of the background wind conditions on the dispersion of the local traffic-related NO_x, we found that a stronger background wind speed lowered both the overall level and spatial

variability of pollution. When the background wind was perpendicular to the axes of most streets in the domain, more severe NO_x pollution and a higher spatial heterogeneity at the pedestrian level were observed.

Our results showed that differences in the ventilation conditions and emissions could lead to a high spatial heterogeneity of the air pollutant concentration at the pedestrian level in urban environments. To accurately measure human exposure to pollution, future urban air quality studies should employ models such as the UTAP model that can differentiate the various concentrations at the street scale without being too computationally costly.

Declaration of competing interest

The authors declare that they have no known competing financial interests or personal relationships that could have appeared to influence the work reported in this paper.

CRediT authorship contribution statement

Xiangwen Fu: Methodology, Software, Formal analysis, Investigation, Writing - original draft. **Songlin Xiang:** Investigation. **Ying Liu:** Writing - review & editing. **Junfeng Liu:** Conceptualization, Writing - review & editing. **Jun Yu:** Investigation. **Denise L. Mauzerall:** Writing - review & editing. **Shu Tao:** Writing - review & editing.

Acknowledgments

This work was supported by funding from the National Key Research and Development Program of China [No. 2016YFC0206202], the National Natural Science Foundation of China (under award nos. 41671491 and 41821005), the Newton Advanced Fellowship (NAFR2180103), and the Science, Technology, and Environmental Policy (STEP) Program of the Woodrow Wilson School of Public and International Affairs at Princeton University.

Appendix A. Supplementary data

Supplementary data to this article can be found online at https://doi.org/10.1016/j.envpol.2020.114390.

References

Abhijith, K.V., Kumar, P., Gallagher, J., McNabola, A., Baldauf, R., Pilla, F., Broderick, B., Di Sabatino, S., Pulvirenti, B., 2017. Air pollution abatement performances of green infrastructure in open road and built-up street canyon environments – a review. Atmos. Environ. 162, 71–86. https://doi.org/10.1016/j.atmosenv.2017.05.014.

Apte, J.S., Messier, K.P., Gani, S., Brauer, M., Kirchstetter, T.W., Lunden, M.M., Marshall, J.D., Portier, C.J., Vermeulen, R.C.H., Hamburg, S.P., 2017. High-resolution air pollution mapping with google street view cars: exploiting big data. Environ. Sci. Technol. 51, 6999–7008. https://doi.org/10.1021/acs.est.7b00891.

Aristodemou, E., Boganegra, L.M., Mottet, L., Pavlidis, D., Constantinou, A., Pain, C., Robins, A., ApSimon, H., 2018. How tall buildings affect turbulent air flows and dispersion of pollution within a neighbourhood. Environ. Pollut. 233, 782–796. https://doi.org/10.1016/j.envpol.2017.10.041.

Baratian-Ghorghi, Z., Kaye, N.B., 2013. The effect of canyon aspect ratio on flushing of dense pollutants from an isolated street canyon. Sci. Total Environ. 443, 112–122. https://doi.org/10.1016/j.scitotenv.2012.10.064.

Barlage, M., Miao, S., Chen, F., 2016. Impact of physics parameterizations on high-resolution weather prediction over two Chinese megacities. J. Geophys. Res. Atmos. 121, 4487–4498. https://doi.org/10.1002/2015JD024450.

Barnes, M.J., Brade, T.K., MacKenzie, A.R., Whyatt, J.D., Carruthers, D.J., Stocker, J., Cai, X., Hewitt, C.N., 2014. Spatially-varying surface roughness and ground-level air quality in an operational dispersion model. Environ. Pollut. Barking Essex 1987 (185), 44–51. https://doi.org/10.1016/j.envpol.2013.09.039.

Batterman, S., Chambliss, S., Isakov, V., 2014. Spatial resolution requirements for traffic-related air pollutant exposure evaluations. Atmos. Environ. 94, 518–528. https://doi.org/10.1016/j.atmosenv.2014.05.065.

Brasseur, O., Declerck, P., Heene, B., Vanderstraeten, P., 2015. Modelling Black Carbon concentrations in two busy street canyons in Brussels using CANSBC. Atmos. Environ. 101, 72–81. https://doi.org/10.1016/j.atmosenv.2014.10.049.

Buchholz, S., Krein, A., Junk, J., Heinemann, G., Hoffmann, L., 2013. Simulation of urban-scale Air pollution patterns in Luxembourg: contributing sources and emission scenarios. Environ. Model. Assess. 18, 271–283. https://doi.org/10.1007/s10666-012-9351-1.

Burnett, R., Chen, H., Szyszkowicz, M., Fann, N., Hubbell, B., Pope, C.A., Apte, J.S., Brauer, M., Cohen, A., Weichenthal, S., Coggins, J., Di, Q., Brunekreef, B., Frostad, J., Lim, S.S., Kan, H., Walker, K.D., Thurston, G.D., Hayes, R.B., Lim, C.C., Turner, M.C., Jerrett, M., Krewski, D., Gapstur, S.M., Diver, W.R., Ostro, B., Goldberg, D., Crouse, D.L., Martin, R.V., Peters, P., Pinault, L., Tjepkema, M., Donkelaar, A., van Villeneuve, P.J., Miller, A.B., Yin, P., Zhou, M., Wang, L., Janssen, N.A.H., Marra, M., Atkinson, R.W., Tsang, H., Thach, T.Q., Cannon, J.B., Allen, R.T., Hart, J.E., Laden, F., Cesaroni, G., Forastiere, F., Weinmayr, G., Jaensch, A., Nagel, G., Concin, H., Spadaro, J.V., 2018. Global estimates of mortality associated with long-term exposure to outdoor fine particulate matter. Proc. Natl. Acad. Sci. Unit. States Am. 115, 9592–9597. https://doi.org/10.1073/pnas.1803222115.

Carpentieri, M., Robins, A.G., Baldi, S., 2009. Three-dimensional mapping of air flow at an urban canyon intersection. Bound.-Layer Meteorol. 133, 277–296. https://doi.org/10.1007/s10546-009-9425-z.

Chang, J.C., Hanna, S.R., 2004. Air quality model performance evaluation. Meteorol. Atmos. Phys. 87, 167–196. https://doi.org/10.1007/s00703-003-0070-7.

Chen, F., Kusaka, H., Bornstein, R., Ching, J., Grimmond, C.S.B., Grossman-Clarke, S., Loridan, T., Manning, K.W., Martilli, A., Miao, S., Sailor, D., Salamanca, F.P., Taha, H., Tewari, M., Wang, X., Wyszogrodzki, A.A., Zhang, C., 2011. The integrated WRF/urban modelling system: development, evaluation, and applications to urban environmental problems. Int. J. Climatol. 31, 273–288. https://doi.org/10.1002/joc.2158.

Chen, G., Zhou, Y., Cheng, S., Yang, X., Wang, X., 2016. Air pollutant emission inventory and impact of typical industries on PM2. 5 in chengde (in Chinese). Environ. Sci. 37, 4069–4079.

Cheshmehzangi, A., 2016. Multi-spatial environmental performance evaluation towards integrated urban design: a procedural approach with computational simulations. J. Clean. Prod. 139, 1085–1093. https://doi.org/10.1016/j.jclepro.2016.08.151.

Fallah-Shorshani, M., Shekarrizfard, M., Hatzopoulou, M., 2017a. Integrating a street-canyon model with a regional Gaussian dispersion model for improved characterisation of near-road air pollution. Atmos. Environ. 153, 21–31. https://doi.org/10.1016/j.atmosenv.2017.01.006.

Fallah-Shorshani, M., Shekarrizfard, M., Hatzopoulou, M., 2017b. Evaluation of regional and local atmospheric dispersion models for the analysis of traffic-related air pollution in urban areas. Atmos. Environ. 167, 270–282. https://doi.org/10.1016/j.atmosenv.2017.08.025.

Farrell, W.J., Deville Cavellin, L., Weichenthal, S., Goldberg, M., Hatzopoulou, M., 2015. Capturing the urban canyon effect on particle number concentrations across a large road network using spatial analysis tools. Build. Environ. 92, 328–334. https://doi.org/10.1016/j.buildenv.2015.05.004.

Forehead, H., Huynh, N., 2018. Review of modelling air pollution from traffic at street-level - the state of the science. Environ. Pollut. 241, 775–786. https://doi.org/10.1016/j.envpol.2018.06.019.

Fu, X., Liu, J., Ban-Weiss, G.A., Zhang, J., Huang, X., Ouyang, B., Popoola, O., Tao, S., 2017. Effects of canyon geometry on the distribution of traffic-related air pollution in a large urban area: implications of a multi-canyon air pollution dispersion model. Atmos. Environ. 165, 111–121. https://doi.org/10.1016/j.atmosenv.2017.06.031.

Gallagher, J., 2016. A modelling exercise to examine variations of NOx concentrations on adjacent footpaths in a street canyon: the importance of accounting for wind conditions and fleet composition. Sci. Total Environ. 550, 1065–1074. https://doi.org/10.1016/j.scitotenv.2016.01.096.

Gu, Z.-L., Zhang, Y.-W., Cheng, Y., Lee, S.-C., 2011. Effect of uneven building layout on air flow and pollutant dispersion in non-uniform street canyons. Build. Environ. 46, 2657–2665. https://doi.org/10.1016/j.buildenv.2011.06.028.

Hang, J., Luo, Z., Wang, X., He, L., Wang, B., Zhu, W., 2017. The influence of street layouts and viaduct settings on daily carbon monoxide exposure and intake fraction in idealized urban canyons. Environ. Pollut. 220, 72–86. https://doi.org/10.1016/j.envpol.2016.09.024.

Hankey, S., Lindsey, G., Marshall, J.D., 2017. Population-level exposure to particulate air pollution during active travel: planning for low-exposure, health-promoting cities. Environ. Health Perspect. 125, 527–534. https://doi.org/10.1289/EHP442.

Hoek, G., Beelen, R., de Hoogh, K., Vienneau, D., Gulliver, J., Fischer, P., Briggs, D., 2008. A review of land-use regression models to assess spatial variation of outdoor air pollution. Atmos. Environ. 42, 7561–7578. https://doi.org/10.1016/j.atmosenv.2008.05.057.

Jiang, L., Bai, L., 2018. Spatio-temporal characteristics of urban air pollution and their causal relationships: evidence from Beijing and its neighboring cities. Sci. Rep. 8, 1279. https://doi.org/10.1038/s41598-017-18107-1.

Jiang, W., Sun, J., Cao, W., Jiang, R., 2004. Air Pollution Meteorology. In: Chinese), second ed. China Meterological Press.

Khan, J., Kakosimos, K., Raaschou-Nielsen, O., Brandt, J., Jensen, S.S., Ellermann, T., Ketzel, M., 2019. Development and performance evaluation of new AirGIS – a GIS based air pollution and human exposure modelling system. Atmos. Environ. 198, 102–121. https://doi.org/10.1016/j.atmosenv.2018.10.036.

Kimbrough, S., Chris Owen, R., Snyder, M., Richmond-Bryant, J., 2017. NO to NO2 conversion rate analysis and implications for dispersion model chemistry

methods using Las Vegas, Nevada near-road field measurements. Atmos. Environ. 165, 23–34. https://doi.org/10.1016/j.atmosenv.2017.06.027.
Krecl, P., Targino, A.C., Johansson, C., Ström, J., 2015. Characterisation and source apportionment of submicron particle number size distributions in a busy street canyon. Aerosol Air Qual. Res. 15, 220–233. https://doi.org/10.4209/aaqr.2014.06.0108.
Kwak, K.-H., Baik, J.-J., Ryu, Y.-H., Lee, S.-H., 2015. Urban air quality simulation in a high-rise building area using a CFD model coupled with mesoscale meteorological and chemistry-transport models. Atmos. Environ. 100, 167–177. https://doi.org/10.1016/j.atmosenv.2014.10.059.
Kwak, K.-H., Lee, S.-H., Seo, J.M., Park, S.-B., Baik, J.-J., 2016. Relationship between rooftop and on-road concentrations of traffic-related pollutants in a busy street canyon: ambient wind effects. Environ. Pollut., Special Issue: Urban Health and Wellbeing 208, 185–197. https://doi.org/10.1016/j.envpol.2015.07.030.
Lateb, M., Meroney, R.N., Yataghene, M., Fellouah, H., Saleh, F., Boufadel, M.C., 2016. On the use of numerical modelling for near-field pollutant dispersion in urban environments–A review. Environ. Pollut. Barking Essex 1987 (208), 271–283. https://doi.org/10.1016/j.envpol.2015.07.039.
Lazić, L., Urošević, M.A., Mijić, Z., Vuković, G., Ilić, L., 2016. Traffic contribution to air pollution in urban street canyons: integrated application of the OSPM, moss biomonitoring and spectral analysis. Atmos. Environ. 141, 347–360. https://doi.org/10.1016/j.atmosenv.2016.07.008.
Li, M., Wang, T., Xie, M., Zhuang, B., Li, S., Han, Y., Song, Y., Cheng, N., 2017. Improved meteorology and ozone air quality simulations using MODIS land surface parameters in the Yangtze River Delta urban cluster, China. J. Geophys. Res. Atmos. 122, 3116–3140. https://doi.org/10.1002/2016JD026182.
Li, X.-X., Britter, R.E., Norford, L.K., Koh, T.-Y., Entekhabi, D., 2012. Flow and pollutant transport in urban street canyons of different aspect ratios with ground heating: large-eddy simulation. Bound.-Layer Meteorol. 142, 289–304. https://doi.org/10.1007/s10546-011-9670-9.
Li, Z., Fung, J.C.H., Lau, A.K.H., 2018. High spatiotemporal characterization of on-road PM2.5 concentrations in high-density urban areas using mobile monitoring. Build. Environ. 143, 196–205. https://doi.org/10.1016/j.buildenv.2018.07.014.
Liu, J., Mauzerall, D.L., Chen, Q., Zhang, Q., Song, Y., Peng, W., Klimont, Z., Qiu, X., Zhang, S., Hu, M., Lin, W., Smith, K.R., Zhu, T., 2016. Air pollutant emissions from Chinese households: a major and underappreciated ambient pollution source. Proc. Natl. Acad. Sci. Unit. States Am. 113, 7756–7761. https://doi.org/10.1073/pnas.1604537113.
Maronga, B., Gryschka, M., Heinze, R., Hoffmann, F., Kanani-Sühring, F., Keck, M., Ketelsen, K., Letzel, M.O., Sühring, M., Raasch, S., 2015. The Parallelized Large-Eddy Simulation Model (PALM) version 4.0 for atmospheric and oceanic flows: model formulation, recent developments, and future perspectives. Geosci. Model Dev. 8, 2515–2551. https://doi.org/10.5194/gmd-8-2515-2015.
Messier, K.P., Chambliss, S.E., Gani, S., Alvarez, R., Brauer, M., Choi, J.J., Hamburg, S.P., Kerckhoffs, J., LaFranchi, B., Lunden, M.M., Marshall, J.D., Portier, C.J., Roy, A., Szpiro, A.A., Vermeulen, R.C.H., Apte, J.S., 2018. Mapping air pollution with google street view cars: efficient approaches with mobile monitoring and land use regression. Environ. Sci. Technol. 52, 12563–12572. https://doi.org/10.1021/acs.est.8b03395.
Michioka, T., Sato, A., Sada, K., 2013. Large-eddy simulation coupled to mesoscale meteorological model for gas dispersion in an urban district. Atmos. Environ. 75, 153–162. https://doi.org/10.1016/j.atmosenv.2013.04.017.
Park, S.-B., Baik, J.-J., Han, B.-S., 2015a. Large-eddy simulation of turbulent flow in a densely built-up urban area. Environ. Fluid Mech. 15, 235–250. https://doi.org/10.1007/s10652-013-9306-3.
Park, S.-B., Baik, J.-J., Lee, S.-H., 2015b. Impacts of mesoscale wind on turbulent flow and ventilation in a densely built-up urban area. J. Appl. Meteorol. Climatol. 54, 811–824. https://doi.org/10.1175/JAMC-D-14-0044.1.
Patterson, R.F., Harley, R.A., 2019. Evaluating near-roadway concentrations of diesel-related air pollution using RLINE. Atmos. Environ. 199, 244–251. https://doi.org/10.1016/j.atmosenv.2018.11.016.
Pattinson, W., Longley, I., Kingham, S., 2014. Using mobile monitoring to visualise diurnal variation of traffic pollutants across two near-highway neighbourhoods. Atmos. Environ. 94, 782–792. https://doi.org/10.1016/j.atmosenv.2014.06.007.
Patton, A.P., Milando, C., Durant, J.L., Kumar, P., 2017. Assessing the suitability of multiple dispersion and land use regression models for urban traffic-related ultrafine particles. Environ. Sci. Technol. 51, 384–392. https://doi.org/10.1021/acs.est.6b04633.
Patton, A.P., Perkins, J., Zamore, W., Levy, J.I., Brugge, D., Durant, J.L., 2014. Spatial and temporal differences in traffic-related air pollution in three urban neighborhoods near an interstate highway. Atmos. Environ. 99, 309–321. https://doi.org/10.1016/j.atmosenv.2014.09.072.
Pospisil, J., Jicha, M., 2017. Influence of vehicle-induced turbulence on pollutant dispersion in street canyon and adjacent urban area. Int. J. Environ. Pollut. 62, 89. https://doi.org/10.1504/IJEP.2017.089400.
Qin, Y., Wagner, F., Scovronick, N., Peng, W., Yang, J., Zhu, T., Smith, K.R., Mauzerall, D.L., 2017. Air quality, health, and climate implications of China's synthetic natural gas development. Proc. Natl. Acad. Sci. Unit. States Am. 114, 4887–4892. https://doi.org/10.1073/pnas.1703167114.
Schraufnagel, D.E., Balmes, J.R., Cowl, C.T., De Matteis, S., Jung, S.-H., Mortimer, K., Perez-Padilla, R., Rice, M.B., Riojas-Rodriguez, H., Sood, A., Thurston, G.D., To, T., Vanker, A., Wuebbles, D.J., 2019a. Air pollution and noncommunicable diseases: a review by the forum of international respiratory societies' environmental committee, Part 1: the damaging effects of air pollution. Chest 155, 409–416. https://doi.org/10.1016/j.chest.2018.10.042.
Schraufnagel, D.E., Balmes, J.R., Cowl, C.T., De Matteis, S., Jung, S.-H., Mortimer, K., Perez-Padilla, R., Rice, M.B., Riojas-Rodriguez, H., Sood, A., Thurston, G.D., To, T., Vanker, A., Wuebbles, D.J., 2019b. Air pollution and noncommunicable diseases: a review by the forum of international respiratory societies' environmental committee, Part 2: air pollution and organ systems. Chest 155, 417–426. https://doi.org/10.1016/j.chest.2018.10.041.
Silver, J.D., Ketzel, M., Brandt, J., 2013. Dynamic parameter estimation for a street canyon air quality model. Environ. Model. Software 47, 235–252. https://doi.org/10.1016/j.envsoft.2013.05.012.
Solazzo, E., Vardoulakis, S., Cai, X., 2011. A novel methodology for interpreting air quality measurements from urban streets using CFD modelling. Atmos. Environ. 45, 5230–5239. https://doi.org/10.1016/j.atmosenv.2011.05.022.
Soulhac, L., Lamaison, G., Cierco, F.-X., Ben Salem, N., Salizzoni, P., Mejean, P., Armand, P., Patryl, L., 2016. SIRANERISK: modelling dispersion of steady and unsteady pollutant releases in the urban canopy. Atmos. Environ. 140, 242–260. https://doi.org/10.1016/j.atmosenv.2016.04.027.
Soulhac, L., Salizzoni, P., Cierco, F.-X., Perkins, R., 2011. The model SIRANE for atmospheric urban pollutant dispersion; part I, presentation of the model. Atmos. Environ. 45, 7379–7395. https://doi.org/10.1016/j.atmosenv.2011.07.008.
Su, H., Wang, Z., Zhu, B., Yin, Y., 2010. Numerical simulation of the SO2 and NO2 dry deposition in Beijing under stagnant weather conditions during the Beijing Olympic games period (in Chinese). Clim. Environ. Res. 15, 636–642.
Targino, A.C., Gibson, M.D., Krecl, P., Rodrigues, M.V.C., dos Santos, M.M., de Paula Corrêa, M., 2016. Hotspots of black carbon and PM2.5 in an urban area and relationships to traffic characteristics. Environ. Pollut. 218, 475–486. https://doi.org/10.1016/j.envpol.2016.07.027.
Targino, A.C., Krecl, P., Danziger Filho, J.E., Segura, J.F., Gibson, M.D., 2018. Spatial variability of on-bicycle black carbon concentrations in the megacity of São Paulo: a pilot study. Environ. Pollut. Barking Essex 1987 (242), 539–543. https://doi.org/10.1016/j.envpol.2018.07.003.
Thaker, P., Gokhale, S., 2016. The impact of traffic-flow patterns on air quality in urban street canyons. Environ. Pollut., Special Issue: Urban Health and Wellbeing 208, 161–169. https://doi.org/10.1016/j.envpol.2015.09.004.
Vardoulakis, S., Fisher, B.E.A., Pericleous, K., Gonzalez-Flesca, N., 2003. Modelling air quality in street canyons: a review. Atmos. Environ. 37, 155–182. https://doi.org/10.1016/S1352-2310(02)00857-9.
Venegas, L.E., Mazzeo, N.A., Dezzutti, M.C., 2014. A simple model for calculating air pollution within street canyons. Atmos. Environ. 87, 77–86. https://doi.org/10.1016/j.atmosenv.2014.01.005.
Wang, A., Fallah-Shorshani, M., Xu, J., Hatzopoulou, M., 2016a. Characterizing near-road air pollution using local-scale emission and dispersion models and validation against in-situ measurements. Atmos. Environ. 142, 452–464. https://doi.org/10.1016/j.atmosenv.2016.08.020.
Wang, L., Zhang, Y., Wang, K., Zheng, B., Zhang, Q., Wei, W., 2016b. Application of weather research and forecasting model with chemistry (WRF/chem) over northern China: sensitivity study, comparative evaluation, and policy implications. Atmos. Environ., Air Pollution in the Beijing – Tianjin – Hebei (BTH) region, China 124, 337–350. https://doi.org/10.1016/j.atmosenv.2014.12.052.
Wang, X., Lei, H., Han, Z., Zhou, D., Shen, Z., Zhang, H., Zhu, H., Bao, Y., 2019. Three-dimensional delayed detached-eddy simulation of wind flow and particle dispersion in the urban environment. Atmos. Environ. 201, 173–189. https://doi.org/10.1016/j.atmosenv.2019.01.004.
Weissert, L.F., Salmond, J.A., Miskell, G., Alavi-Shoshtari, M., Williams, D.E., 2018. Development of a microscale land use regression model for predicting NO2 concentrations at a heavy trafficked suburban area in Auckland, NZ. Sci. Total Environ. 619–620, 112–119. https://doi.org/10.1016/j.scitotenv.2017.11.028.
Yang, J., Li, X., Peng, W., Wagner, F., Mauzerall, D.L., 2018. Climate, air quality and human health benefits of various solar photovoltaic deployment scenarios in China in 2030. Environ. Res. Lett. 13, 064002 https://doi.org/10.1088/1748-9326/aabe99.
Zhang, X., Craft, E., Zhang, K., 2017. Characterizing spatial variability of air pollution from vehicle traffic around the Houston Ship Channel area. Atmos. Environ. 161, 167–175. https://doi.org/10.1016/j.atmosenv.2017.04.032.
Zhong, J., Cai, X.-M., Bloss, W.J., 2017. Large eddy simulation of reactive pollutants in a deep urban street canyon: coupling dynamics with O3-NOx-VOC chemistry. Environ. Pollut. 224, 171–184. https://doi.org/10.1016/j.envpol.2017.01.076.
Zhong, J., Cai, X.-M., Bloss, W.J., 2015. Modelling the dispersion and transport of reactive pollutants in a deep urban street canyon: using large-eddy simulation. Environ. Pollut. 200, 42–52. https://doi.org/10.1016/j.envpol.2015.02.009.
Zhong, J., Nikolova, I., Cai, X., MacKenzie, A.R., Harrison, R.M., 2018. Modelling traffic-induced multicomponent ultrafine particles in urban street canyon compartments: factors that inhibit mixing. Environ. Pollut. 238, 186–195. https://doi.org/10.1016/j.envpol.2018.03.002.
Zhou, S., Lin, R., 2019. Spatial-temporal heterogeneity of air pollution: the relationship between built environment and on-road PM2.5 at micro scale. Transport. Res. Part Transp. Environ. 76, 305–322. https://doi.org/10.1016/j.trd.2019.09.004.